A METHOD FOR COMPUTING BOUNDARY-LAYER FLOWS, INCLUDING NORMAL PRESSURE GRADIENT AND LONGITUDINAL CURVATURE EFFECTS

Arloe W. Mayne, Jr.
ARO, Inc.

VON KÁRMÁN GAS DYNAMICS FACILITY
ARNOLD ENGINEERING DEVELOPMENT CENTER
AIR FORCE SYSTEMS COMMAND
ARNOLD AIR FORCE STATION, TENNESSEE 37389

April 1975

Final Report for Period September 1973 — August 1974

Prepared for

DIRECTORATE OF TECHNOLOGY
ARNOLD ENGINEERING DEVELOPMENT CENTER
ARNOLD AIR FORCE STATION, TENNESSEE 37389

This report has been reviewed by the Information Office (OI) and is releasable to the National Technical Information Service (NTIS). At NTIS, it will be available to the general public, including foreign nations.
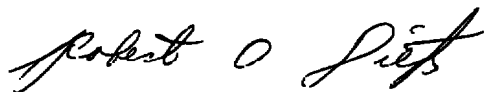
APPROVAL STATEMENT

This technical report has been reviewed and is approved for publication.

FOR THE COMMANDER

ELTON R. THOMPSON
Research and Development
   Division
Directorate of Technology

ROBERT O. DIETZ
Director of Technology

UNCLASSIFIED

REPORT DOCUMENTATION PAGE		READ INSTRUCTIONS BEFORE COMPLETING FORM
1 REPORT NUMBER AEDC-TR-75-21	2 GOVT ACCESSION NO.	3 RECIPIENT'S CATALOG NUMBER
4. TITLE (and Subtitle) A METHOD FOR COMPUTING BOUNDARY-LAYER FLOWS, INCLUDING NORMAL PRESSURE GRADIENT AND LONGITUDINAL CURVATURE EFFECTS		5 TYPE OF REPORT & PERIOD COVERED Final Report-September 1973 to August 1974
		6. PERFORMING ORG. REPORT NUMBER
7 AUTHOR(s) Arloe W. Mayne, Jr., ARO, Inc.		8 CONTRACT OR GRANT NUMBER(s)
9 PERFORMING ORGANIZATION NAME AND ADDRESS Arnold Engineering Development Center(XO) Arnold Air Force Station, Tennessee 37389		10. PROGRAM ELEMENT, PROJECT, TASK AREA & WORK UNIT NUMBERS Program Element 65807F
11. CONTROLLING OFFICE NAME AND ADDRESS Arnold Engineering Development Center (DYFS) Arnold Air Force Station, Tennessee 37389		12. REPORT DATE April 1975
		13 NUMBER OF PAGES 34
14 MONITORING AGENCY NAME & ADDRESS(if different from Controlling Office)		15. SECURITY CLASS. (of this report) UNCLASSIFIED
		15a. DECLASSIFICATION/DOWNGRADING SCHEDULE N/A

16 DISTRIBUTION STATEMENT (of this Report)

Approved for public release; distribution unlimited.

17 DISTRIBUTION STATEMENT (of the abstract entered in Block 20, if different from Report)

18 SUPPLEMENTARY NOTES

Available in DDC

19 KEY WORDS (Continue on reverse side if necessary and identify by block number)

methodology
computations
boundary-layer flow
pressure (normal)

gradients
curvature (longitudinal)
equations

20. ABSTRACT (Continue on reverse side if necessary and identify by block number)

A method is presented for computing laminar and turbulent boundary-layer flows, including normal pressure gradient and longitudinal curvature as well as compressibility, transverse curvature, and other effects. The governing equations are transformed using the ω^2 transformation to a von Mises form and solved using an implicit finite-difference scheme. The

DD FORM 1473 1 JAN 73   EDITION OF 1 NOV 65 IS OBSOLETE

UNCLASSIFIED

20. ABSTRACT (Continued)

method is validated by comparing results with experimental data
and results of other methods of computation.

PREFACE

The work reported herein was conducted by the Arnold Engineering Development Center (AEDC), Air Force Systems Command (AFSC), under Program Element 65807F. The results of the research presented were obtained by ARO, Inc. (a subsidiary of Sverdrup & Parcel and Associates, Inc.), contract operator of AEDC, AFSC, Arnold Air Force Station, Tennessee. The research was conducted from September 1973 to August 1974 under ARO Project Nos. VF403 and V33P, and the manuscript (ARO Control No. ARO-VKF-TR-74-114) was submitted for publication on November 20, 1974.

Appreciation and acknowledgment are extended to Mr. E. O. Marchand, ARO, Inc., for performing the inviscid flow and fully viscous shock layer computations used in this investigation.

1

CONTENTS

ILLUSTRATIONS

TABLES

1.0 INTRODUCTION

One of the most widely used methods for calculating boundary-layer flows is that developed originally by Patankar and Spalding (Ref. 1). This has been largely due to the versatility and ease of application of the method. At the Arnold Engineering Development Center, the method of Patankar and Spalding has been applied to a wide variety of problems, ranging from laminar incompressible flows to turbulent supersonic flows (e.g., Refs. 2 and 3). As originally conceived, this method was capable of treating both laminar and turbulent boundary layers and included the transverse curvature effect for both internal (nozzle or channel) and external axisymmetric flows. Each user of the method of Patankar and Spalding has, of course, styled it to his particular taste, and a number of significant modifications have been made. These include the addition of equilibrium dissociating air thermodynamic and transport properties, the treatment of entropy layer swallowing in computing supersonic and hypersonic flow over blunt-nosed bodies, and extension of the basic method to treat the three-dimensional boundary-layer flow in the windward symmetry plane of an axisymmetric body at angle of attack (Refs. 4 and 5).

The purpose of this report is to present a recently developed method for computing boundary-layer flows. Although the method to be presented is derived from the work of Patankar and Spalding, there are a number of significant deviations from and extensions to their work. For this reason, much of the success of the present method must be attributed to the previous efforts of Patankar and Spalding, while any blame for shortcomings of the modified computation must be borne by the present author.

One of the primary contributions of Patankar and Spalding was the introduction of the ω coordinate for the direction normal to the body surface. This is a normalized von Mises coordinate which varies from zero at the body surface to unity at the outer edge of the boundary layer. The simple ω coordinate has, however, certain shortcomings: one is the singularity of certain derivatives with respect to ω when evaluated at the body surface, and a second is the necessity for predicting the rate of change of the stream function along the outer edge of the boundary layer as the flow proceeds. The first of these can be eliminated, as has been done by Landis (Ref. 6), by adopting a so-called ω^2 transformation, and this approach has been used in the present work. Not only does the use of the ω^2 transformation eliminate the aesthetically distasteful singularity

5

mentioned above, it also yields more accurate numerical results according to Denny and Landis (Ref. 7). Unfortunately, the problem of determining the growth rate of the stream function has no patent solution, but through careful monitoring and controls it can be adequately determined.

A second difference between the present work and that of Ref. 1 is that an option for considering the effects of longitudinal curvature and the variation of the static pressure in the direction normal to the body surface has been included in the method presented herein. The use of a difference scheme derived from Taylor series truncation is another major difference between the method described in this report and that presented in Ref. 1. Because of the coupling of the normal and longitudinal pressure gradients, and because of the numerical scheme used for turbulent flows, the resulting finite-difference solution method is an iterative one, in contrast to the non-iterative method of Ref. 1.

The next section presents the governing equations and the finite-difference method which is employed in solving them, and in the succeeding section are given the results of a variety of test calculations which have been performed, including internal and external flows and flows with significant normal pressure gradients.

2.0 GOVERNING EQUATIONS AND METHOD OF SOLUTION

In this section are presented the governing equations for compressible boundary-layer flow and the finite-difference method used to solve these equations. The boundary-layer equations include transverse curvature, longitudinal curvature, and normal pressure gradient effects. The equations are given first in x-y surface coordinates, and later the transformation to x-ω coordinates (using the ω^2 transformation) is given.

In this investigation, the stagnation point form of the boundary-layer equations were derived and solved. To the author's knowledge this has not previously been done using the ω or ω^2 transformation, and for that reason, the stagnation point form of the boundary-layer equations using the ω^2 transformation is also presented in this report.

The results which are given in the next section are all for a thermally and calorically perfect gas; however, the method which has been developed is also capable of treating the flow of equilibrium dissociating air. This has been achieved by using the thermodynamic and transport

6

property correlations of Cohen (Ref. 8) which have been faired into perfect-gas, constant-Prandtl number, Sutherland-viscosity relations at lower temperatures. For the case of turbulent flows, a two-layer eddy-transport property formulation was used; a streamwise inter-mittency factor was used to treat transition from laminar to turbulent flow.

2.1 BOUNDARY-LAYER EQUATIONS AND TRANSPORT LAWS

The boundary-layer equations which have been used are essentially those given by Maslen (Ref. 9), except that the Prandtl number has not been assumed to be constant and is, therefore, included within the y derivative in the energy equation. When both longitudinal and transverse curvature terms are retained, the boundary-layer equations have the following form:

continuity:

$$\frac{\partial}{\partial x}(\rho u r^j) + \frac{\partial}{\partial y}[(1 + \kappa y)\rho v r^j] = 0 \tag{1}$$

x-momentum:

$$\rho u \frac{\partial u}{\partial x} + \rho v(1 + \kappa y)\frac{\partial u}{\partial y} + \rho u v \kappa = -\frac{\partial p}{\partial x} + \frac{1}{r^j}\frac{\partial}{\partial y}\left[\mu r^j(1 + \kappa y)\frac{\partial u}{\partial y}\right] - \kappa u \frac{\partial \mu}{\partial y} \tag{2}$$

y-momentum:

$$\frac{\partial p}{\partial y} = \kappa \rho u^2 \tag{3}$$

energy:

$$\rho u \frac{\partial H}{\partial x} + \rho v(1 + \kappa y)\frac{\partial H}{\partial y} = -\frac{\kappa \partial(\mu u^2)}{\partial y} + \frac{1}{r^j}\frac{\partial}{\partial y}\left[\frac{\mu r^j}{Pr}(1 + \kappa y)\frac{\partial H}{\partial y} + \frac{Pr - 1}{Pr}\mu r^j(1 + \kappa y)\frac{\partial(u^2/2)}{\partial y}\right] \tag{4}$$

These equations are similar to those used by Back (Ref. 10), although he treated some of the curvature terms differently. In these equations u and v are velocity components parallel and normal to the surface (in the x and y directions), and κ is the surface curvature (see Fig. 1). The κ is the reciprocal of the longitudinal radius of curvature R, except that it is counted negative for concave surfaces and positive for convex

surfaces. The power j is +1 for axisymmetric flow and 0 for two-dimensional flow. The r and y are related by

$$r = r_w + iy \cos \phi \qquad (5)$$

where r_w is the transverse radius of the body, ϕ is the body slope, and i is an index which is +1 for external flow, -1 for internal flow, and 0 if transverse curvature is to be neglected.
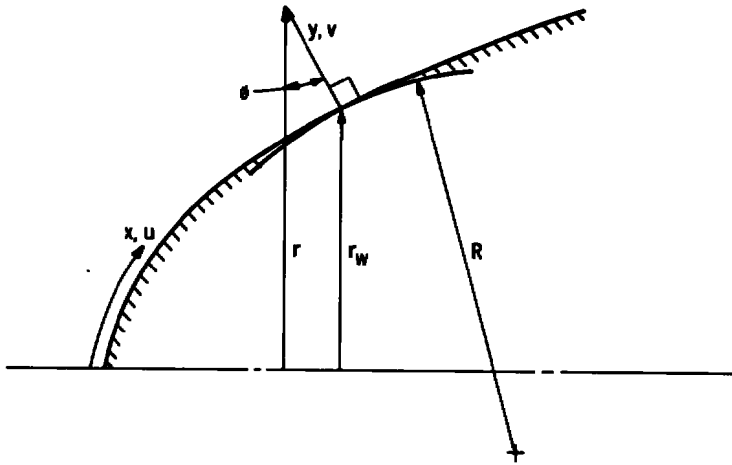
Figure 1. Typical configuration showing coordinates and velocity components.

Boundary conditions (at the surface, subscript w, and outer edge, subscript e) for Eqs. (1) through (4) are as follows:

$$y = 0: \quad v = v_w$$

$$u = 0$$

$$H = H_w \text{ or } \partial H / \partial y = 0$$

$$y = y_e: \quad u = u_e$$

$$p = p_e$$

$$H = H_\infty \qquad (6)$$

Typically, the distribution of static pressure along the body surface, as computed by methods for inviscid flow, is known. Assuming then that Eq. (3) is valid in the inviscid flow region near the body surface, p_e was determined by numerically integrating Eq. (3) from the body surface to the value of the stream function at the outer edge of the boundary layer,

treating the flow as inviscid. This was done while simultaneously determining the variation of u, ρ, etc. in this region by conventional methods, including the treatment of entropy swallowing on blunt bodies in supersonic flow by the method described in Ref. 4. This also resulted in the determination of u_e.

For laminar (molecular) thermodynamic and transport properties, constant specific heats and a Sutherland viscosity law were used for perfect-gas calculations and Cohen's correlations (Ref. 8) mentioned previously were used to obtain properties of equilibrium dissociating air.

In order to treat transitional and turbulent boundary-layer flow, a two-layer eddy-transport property hypothesis and a streamwise intermittency factor, γ, were employed. The independent variables in Eqs. (1) through (4) were treated as time-mean quantities, and the transport properties were treated as follows:

$$\mu = \mu_\ell + \gamma\mu_t \tag{7}$$

$$\frac{\mu}{Pr} = \frac{\mu}{Pr_\ell} + \gamma\frac{\mu_t}{Pr_t} \tag{8}$$

where

$$(\mu_t)_{inner} = \rho k^2 y^2 \left[1 - \exp\left(\frac{-y\sqrt{\tau\rho}}{\mu_\ell A^*}\right)\right]^2 \left|\frac{\partial u}{\partial y}\right| \tag{9}$$

$$(\mu_t)_{outer} = \rho\lambda^2 y_m^2 \left|\frac{\partial u}{\partial y}\right| \tag{10}$$

Equation (9) was used out to the point where $(\mu_t)_{inner} = (\mu_t)_{outer}$, and Eq. (10) was used beyond that. Equations (9) and (10) are those recommended in Ref. 1, and the values used for λ, A^*, and k were 0.09, 26.0, and 0.435, respectively, which are essentially those given in Ref. 1. The y_m is the value of y where $u/u_e = 0.99$.

The intermittency factor determined by Dhawan and Narasimha (Ref. 11) was used; this has the form

$$\gamma = 1 - \exp\left[-3.507\left(\frac{x - x_a}{x_b - x_a}\right)^2\right] \tag{11}$$

where x_a is the value of x at the beginning of transition and x_b the value at the end of transition.

2.2 TRANSFORMATION OF THE GOVERNING EQUATIONS

In order to transform the governing equations, a stream function was defined which satisfies the continuity equation, and then a variable ω was introduced, where ω^2 is a normalized form of the stream function. The stream function ψ is defined by

$$\left(\frac{\partial \psi}{\partial x}\right)_y = - (1 + \kappa y)\rho \, v \, r^j$$

$$\left(\frac{\partial \psi}{\partial y}\right)_x = \rho \, u \, r^j \tag{12}$$

The variable ω is defined by

$$\omega^2 = \frac{\psi - \psi_w}{\psi_e - \psi_w} \tag{13}$$

These were used to obtain the transformation operators

$$\left(\frac{\partial f}{\partial x}\right)_y = \left(\frac{\partial f}{\partial x}\right)_\omega - \left(\frac{\partial f}{\partial \omega}\right)_x \frac{(1 + \kappa y)\rho \, v \, r^j}{2\omega(\psi_e - \psi_w)} - \left(\frac{\partial f}{\partial \omega}\right)_x \frac{\frac{d\psi_w}{dx} + \omega^2\left(\frac{d\psi_e}{dx} - \frac{d\psi_w}{dx}\right)}{2\omega(\psi_e - \psi_w)} \tag{14}$$

$$\left(\frac{\partial f}{\partial y}\right)_x = \frac{\rho \, u \, r^j}{2\omega(\psi_e - \psi_w)} \left(\frac{\partial f}{\partial \omega}\right)_x \tag{15}$$

Equations (14) and (15) can be combined to treat the convective terms of Eqs. (2) and (4), yielding

$$\rho u\left(\frac{\partial f}{\partial x}\right)_y + (1 + \kappa y) \, \rho v\left(\frac{\partial f}{\partial y}\right)_x = \rho u\left(\frac{\partial f}{\partial x}\right)_\omega - \rho u\left(\frac{\partial f}{\partial \omega}\right)_x \frac{\frac{d\psi_w}{dx} + \omega^2\left(\frac{d\psi_e}{dx} - \frac{d\psi_w}{dx}\right)}{2\omega(\psi_e - \psi_w)} \tag{16}$$

Application of Eqs. (14), (15), and (16) to Eqs. (2) and (4) yields the following general form

$$\left(\frac{\partial f}{\partial x}\right)_\omega + a_f\left(\frac{\partial f}{\partial \omega}\right)_x = b_f \frac{\partial}{\partial \omega}\left[c_f\left(\frac{\partial f}{\partial \omega}\right)_x\right]_x + d_f \tag{17}$$

where, for $f = u$

$$a_u = \frac{1}{2\omega}\left[\frac{r_w^j \dot{m}_w'' - \omega^2(r_w^j \dot{m}_w'' - r_e^j \dot{m}_e'')}{PEI}\right]$$

$$b_u = \frac{1}{2\omega}$$

$$c_u = \frac{\rho u \mu \, r^{2j}(1 + \kappa y)}{2\omega \, PEI^2}$$

$$d_u = -v\kappa - \frac{1}{\rho u}\left(\frac{\partial p}{\partial x}\right)_\omega - \left(\frac{\partial p}{\partial \omega}\right)_x \frac{1}{2\omega}\left[\frac{r_w^j \dot{m}_w'' - \omega^2(r_w^j \dot{m}_w'' - r_e^j \dot{m}_e'')}{\rho u \, PEI}\right]$$

$$+ \left(\frac{\partial p}{\partial \omega}\right)_x \frac{(1 + \kappa y)v r^j}{2\omega u \, PEI} - \frac{\kappa u r^j}{2\omega \, PEI}\left(\frac{\partial \mu}{\partial \omega}\right)_x \tag{18}$$

with

$$\frac{d\psi_e}{dx} = -r_e^j \dot{m}_e''$$

$$\frac{d\psi_w}{dx} = -r_w^j \dot{m}_w'' \tag{19}$$

and

$$PEI = \psi_e - \psi_w$$

For the energy equation, where $f = H$,

$$a_H = a_u$$

$$b_H = b_u$$

$$c_H = c_u / Pr$$

$$d_H = \frac{-\kappa r^j}{2\omega \, PEI}\left(\frac{\partial(\mu u^2)}{\partial \omega}\right)_x + \frac{1}{2\omega}\frac{\partial}{\partial \omega}\left[\rho u \mu r^{2j}(1 + \kappa y)\frac{Pr - 1}{Pr}\frac{1}{2\omega \, PEI^2}\left(\frac{\partial(u^2/2)}{\partial \omega}\right)_x\right]_x \tag{20}$$

11

In addition to solving equations of the form of Eq. (17) for u and H, Eq. (3) was integrated from $y = y_e$ to $y = 0$ to obtain the variation of p through the boundary layer, and the definition of the stream function was used to obtain the v component of velocity. To obtain y from ω, the following equation was integrated at a given value of x from $\omega = 0$ to $\omega = 1$

$$y = \int_o^\omega \frac{2\omega \; PEI}{\rho u r^j} \; d\omega$$

(21)

The quantities $\dot{m}_e''$ and $\dot{m}_w''$ introduced in Eqs. (19) were required in order to solve the x-momentum and energy equations; $\dot{m}_w''$ was determined from the surface mass flux which was specified, and $\dot{m}_e''$ was determined in all cases in a manner similar to that used in Ref. 1 for laminar flow, namely by considering the x-momentum equation near the outer edge of the boundary layer. The value so obtained was adjusted to prevent large variations in $\dot{m}_e''$ from step to step in x, and, since $\dot{m}_e''$ controls the extent of the region over which the boundary-layer equations are solved, it was also adjusted to assure that the boundary-layer equations were not being solved over a region of essentially inviscid flow.

For the present application, the primary advantage of the ω coordinate, as opposed to retaining the physical coordinate y, is that the boundary layer always lies in the region $0 \leq \omega \leq 1$, while in terms of y the extent of the region of interest is unknown and generally increases with x. If the variation of p with y were not being considered, the need for a knowledge of v would vanish, and neither the stream function equation nor the continuity equation would need to be solved.

2.3 STAGNATION POINT EQUATIONS

In order to begin the numerical solution of the equations represented by Eq. (17), it is necessary to have initial profiles of u and H as functions of ω. These can be provided from experimental data, approximations, or other sources, as in Refs. 2 and 6 for instance. For the case of flow over a blunt-nosed body, however, the governing equations can be reduced to a two-point boundary-value problem at the stagnation point, the solution of which can provide the initial profiles needed to start the general solution.

In the present work, the stagnation point x-momentum and energy equations were formed by introducing a dependent variable, ζ, where

$$\zeta = u/u_e \tag{22}$$

and then considering the limiting forms which the equations took as x approached zero. A typical term in this treatment is the following:

$$\lim_{x \to 0} \frac{u_e r_w^j}{PEI} = \frac{j+1}{\dot{m}_w'' - \left(\frac{r_e}{r_w}\right)^j \dot{m}_e''} \left(\frac{du_e}{dx}\right)_o \tag{23}$$

where

$$\lim_{x \to 0} \frac{r_e}{r_w} = 1 + \frac{y_e}{r_n}$$

In these equations, $(du_e/dx)_0$ is the stagnation point edge velocity gradient which was evaluated using Euler's equation and a modified Newtonian pressure distribution.

The resulting form of the x-momentum equation at the stagnation point is

$$\overline{a}_u \left(\frac{\partial \zeta}{\partial \omega}\right)_x + \overline{b}_u \frac{\partial}{\partial \omega}\left[\overline{c}_u\left(\frac{\partial \zeta}{\partial \omega}\right)_x\right]_x + \overline{d}_u = 0 \tag{24}$$

where

$$\overline{a}_u = \frac{T_w' \dot{m}_w'' - \omega^2(T_w' \dot{m}_w'' - T_e' \dot{m}_e'')}{2\omega}$$

$$\overline{b}_u = \frac{1}{2\omega}$$

$$\overline{c}_u = \frac{\rho \zeta \mu (1 + \kappa y) T'^2}{2\omega}$$

$$\overline{d}_u = \left(\zeta - \frac{\rho_e}{\rho \zeta}\right)\left(\frac{du_e}{dx}\right)_o + \nu \kappa^2 y + \frac{\dot{m}_e'' \kappa}{\omega^2 \rho \zeta} + \frac{\kappa \zeta}{2\omega} T'\left(\frac{\partial \mu}{\partial \omega}\right)_x \tag{25}$$

and

$$T_w' = \frac{j + 1}{\dot{m}_w'' - \left(1 + \dfrac{y_e}{r_n}\right)^j \dot{m}_e''} \left(\frac{du_e}{dx}\right)_o$$

$$T_e' = \frac{j + 1}{\dfrac{1}{(1 + y_e/r_n)^j} \dot{m}_w'' - \dot{m}_e''} \left(\frac{du_e}{dx}\right)_o$$

$$T' = \frac{j + 1}{\dfrac{1}{(1 + y/r_n)^j} \dot{m}_w'' - \left(\dfrac{1 + y_e/r_n}{1 + y/r_n}\right)^j \dot{m}_e''} \left(\frac{du_e}{dx}\right)_o \tag{26}$$

In obtaining $\bar{d}_u$ the y-momentum equation was converted to x-ω form and used in treating those terms in d_u which included $(\partial p/\partial \omega)_x$ as a coefficient.

Before the limiting form of the energy equation could be developed, it was necessary to multiply the entire equation by u_e. The resulting form of the energy equation at the stagnation point is

$$\bar{a}_H \left(\frac{\partial H}{\partial \omega}\right)_x + \bar{b}_H \frac{\partial}{\partial \omega} \left[\bar{c}_H \left(\frac{\partial H}{\partial \omega}\right)_x\right]_x + \bar{d}_H = 0 \tag{27}$$

where

$$\bar{a}_H = \bar{a}_u$$

$$\bar{b}_H = \bar{b}_u$$

$$\bar{c}_H = \bar{c}_u/Pr$$

$$\bar{d}_H = 0 \tag{28}$$

Application of l'Hospital's rule to the definition of ω, together with the introduction of the definition of ψ yields the following equation for v at the stagnation point

$$v = \frac{1}{(1 + \kappa y)\rho(1 + y/r_n)^j} \left\{\omega^2 \left[(1 + y_e/r_n)^j \dot{m}_e'' - \dot{m}_w''\right] + \dot{m}_w''\right\} \tag{29}$$

Since u = 0 at the stagnation point, the use of Eq. (3) yields a constant static pressure at that location, and at the stagnation point y can be determined from

$$y = \int_0^\omega \frac{2\omega}{\rho \zeta T} \, d\omega$$

(30)

The quantity $\dot{m}_e''$, called the entrainment rate because of its relation to the growth of the stream function due to the entrainment of fluid into the boundary layer, was evaluated at the stagnation point by examining a number of stagnation point boundary-layer solutions and determining that

$$\dot{m}_e'' = -30 \rho_\infty U_\infty' \sqrt{Re_\infty, r_n}$$

(31)

yielded a value which was generally satisfactory.

2.4 FINITE-DIFFERENCE EQUATIONS

In order to solve the coupled partial differential equations for u and H represented by Eq. (17), this equation was replaced by a set of consistent linearized algebraic equations. The set is of tridiagonal form and was solved by means of a standard algorithm which is especially efficient for such forms.

As mentioned previously, in order to solve the finite-difference form of the governing equations at a general x location, it was necessary to have a complete solution at a previous x station. To start the process this initial solution was obtained from experimental data, approximations, or a finite-difference solution of the stagnation point equations. This is indicated schematically in Fig. 2 where x location 1 represents a location where the solution is known and location 2 the location where the solution is to be obtained.

With Eq. (17) in the form

$$\left(\frac{\partial^2 f}{\partial \omega^2}\right)_x + \left[\frac{1}{c_f}\left(\frac{\partial c_f}{\partial \omega}\right)_x - \frac{a_f}{b_f c_f}\right]\left(\frac{\partial f}{\partial \omega}\right)_x - \frac{1}{b_f c_f}\left(\frac{\partial f}{\partial x}\right)_\omega + \frac{d_f}{b_f c_f} = 0$$

(32)

the following difference forms obtained from Taylor series truncation were employed.

15

$$f_{I,2} = f_{I,1} + 0(\Delta x)$$

$$\left(\frac{\partial f}{\partial x}\right)_{I,2} = \frac{f_{I,2} - f_{I,1}}{\Delta x} + 0(\Delta x)$$

$$\left(\frac{\partial f}{\partial \omega}\right)_{I,2} = \frac{f_{I+1,2} - f_{I-1,2}}{\Delta\omega_I^+ + \Delta\omega_I^-} + 0(\Delta\omega)$$

$$\left(\frac{\partial^2 f}{\partial \omega^2}\right)_{I,2} = \frac{2}{\Delta\omega_I^+ + \Delta\omega_I^-}\left(\frac{f_{I+1,2} - f_{I,2}}{\Delta\omega_I^+} + \frac{f_{I-1,2} - f_{I,2}}{\Delta\omega_I^-}\right) + 0(\Delta\omega) \tag{33}$$
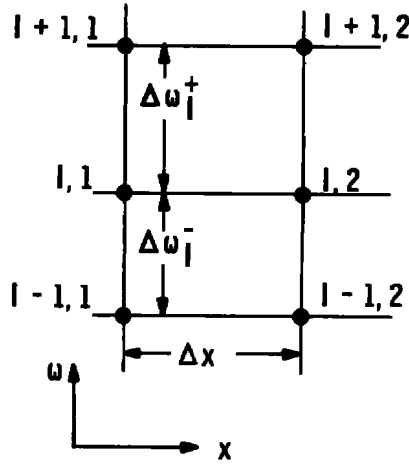
Figure 2. Typical section of finite-difference grid.

Application of Eq. (33) to Eq. (32) yields the following general form for the corresponding finite-difference equation

$$f_{I,2} = A_{f,I}f_{I+1,2} + B_{f,I}f_{I-1,2} - C_{f,I} \tag{34}$$

where

$$A_{f,I} = \frac{1}{D_{f,I}}\left(\frac{2}{(\Delta\omega_I^+ + \Delta\omega_I^-)\Delta\omega_I^+} + \frac{P_{f,I}}{\Delta\omega_I^+ + \Delta\omega_I^-}\right)$$

$$B_{f,I} = \frac{1}{D_{f,I}}\left(\frac{2}{(\Delta\omega_I^+ + \Delta\omega_I^-)\Delta\omega_I^-} - \frac{P_{f,I}}{\Delta\omega_I^+ + \Delta\omega_I^-}\right)$$

16

$$C_{f,I} = \frac{1}{D_{f,I}} \; \frac{1}{b_{f_{I,1}} \; c_{f_{I,1}}} \left(\frac{a_{f_{I,1}}}{\Delta x} + d_{f_{I,1}} \right)$$

$$D_{f,I} = \frac{2}{\Delta\omega_I^+ - \Delta\omega_I^-} \left(\frac{1}{\Delta\omega_I^+} + \frac{1}{\Delta\omega_I^-} \right) + \frac{1}{b_{f_{i,1}} \; c_{f_{I,1}} \; \Delta x}$$

$$P_{f,I} = \frac{1}{c_{f_{I,1}}} \; \frac{c_{f_{I+1,1}} - c_{f_{I-1,1}}}{\Delta\omega_I^+ + \Delta\omega_I^-} - \frac{a_{f_{I,1}}}{b_{f_{I,1}} \; c_{f_{I,1}}} \tag{35}$$

In Eq. (35) it is indicated that a_f, b_f, c_f, and d_f are evaluated at x location 1, and this proved to be a valid and effective treatment for laminar flow problems. For turbulent flow problems, however, difficulty was encountered in the solution. This appeared as an oscillation in the turbulent viscosity and shearing stress from one x location to the next, in the neighborhood of the changeover from the inner-layer viscosity law to the outer-layer law. To alleviate this problem, the value of the viscosity at x location 2 was used in the c_f terms. Since this viscosity is not known beforehand, this treatment necessitates an iteration for the solution at location 2.

For f equal to each of u and H an equation of the form of Eq. (34) can be written for $1 < I < N$, where N is the number of grid points from the surface to the outer edge, including both end points. With the boundary conditions as described previously, the equations represented by Eq. (34) were solved using the standard algorithm for linear tridiagonal systems, as described in Ref. 1. After the values of u and H were determined at x location 2, the thermodynamic and transport properties, p(y), and v(y) were determined. Since iteration was required, for the reason previously discussed, this was done until convergence was attained, and then the whole procedure was repeated at the next x location, with location 1 values having been replaced by location 2 values.

It is noteworthy that the finite-difference grid used required neither Δx nor $\Delta\omega$ to be a constant; in particular, an ω grid was used which caused the point spacing to be much closer near the surface than in the outer part of the boundary layer.

At the stagnation point of a blunt body an iterative finite-difference method was used, employing difference forms for the derivatives with respect to ω as given in Eq. (33). All data except the values of the

dependent variables in the derivatives with respect to ω were taken from initial approximation or previous iteration values and were recomputed after new values for ζ and H were found. The iteration was then repeated until convergence was attained.

3.0 RESULTS OF CALCULATIONS

The general behavior of the solution method described in the previous section was investigated by performing a series of calculations to investigate grid spacing, convergence criteria, and other factors involved in applying the finite-difference technique. It was determined that a practical value for the number of ω grid lines was 50, and the various iterations involved were deemed to be converged when successive values of the variables involved differed no more than 0.05 percent.

All computations performed in this investigation were done in double precision on an IBM Model 370/155 digital computer, using approximately 180,000 bytes of core and 15 minutes of central processor time per case.

3.1 22.5-DEG HYPERBOLOID IN MACH 10 FLOW

One test of the present method was to make comparisons with results obtained in the investigation reported in Ref. 4. The situation was that of the flow of air over a 0.1-ft nose-radius, 22.5-deg, asymptotic half-angle hyperboloid. The free-stream Mach number was 10, and the free-stream Reynolds number based on nose radius was 4,000. The wall-to-free-stream stagnation temperature ratio was 0.2, and the boundary-layer flow was assumed to be laminar. For this case the boundary layer occupies about one-third of the region between the body and the bow shock, and the effects of entropy layer swallowing were shown in Ref. 4 to be significant.

Figures 3, 4, and 5 show comparisons of results from the present method with results from the fully viscous shock layer method of Ref. 12. For this problem, the shock layer method should be the best of all those which are available; however, shock layer methods are currently quite restricted in their range of applicability.
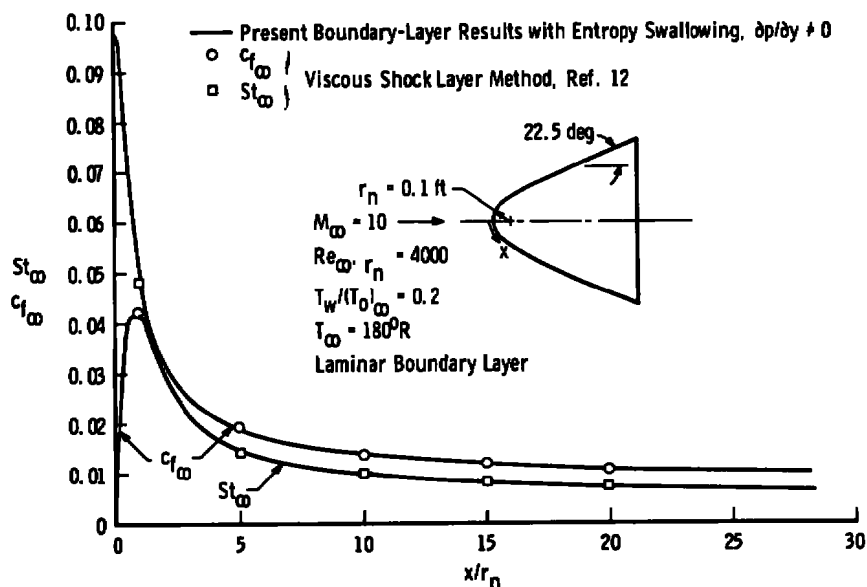
Figure 3. Stanton number and skin friction coefficient distributions on a 22.5-deg hyperboloid in a Mach 10 flow.
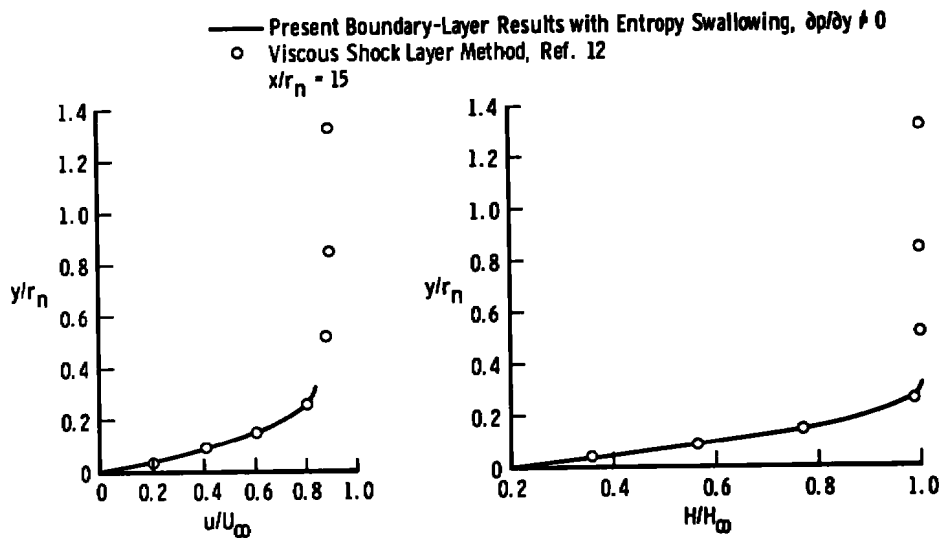

Figure 4. Velocity and total enthalpy profiles at x/r_n = 15 on a 22.5-deg hyperboloid in a Mach 10 flow.
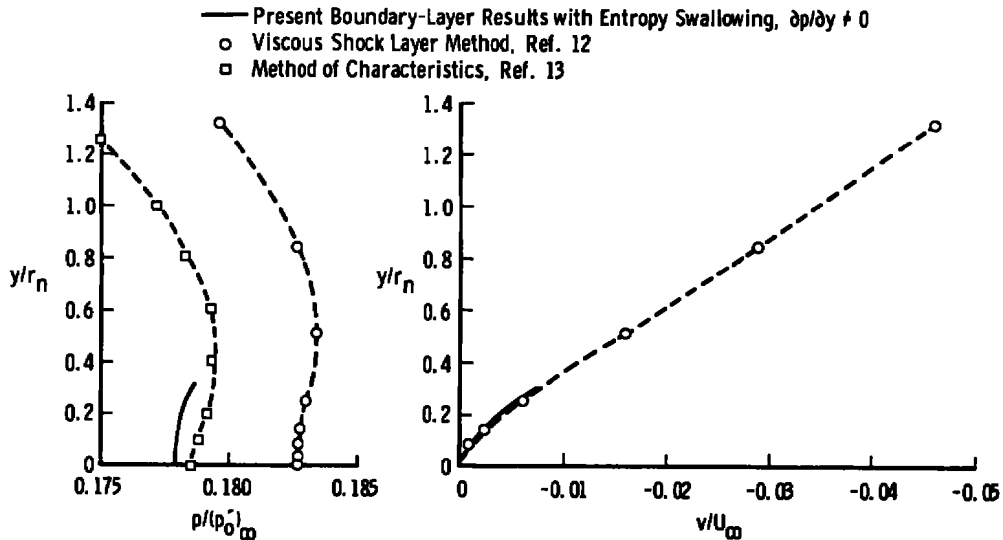
Figure 5. Static pressure and normal velocity profiles at x/r_n = 15
on a 22.5-deg hyperboloid in a Mach 10 flow.

Figure 3 compares Stanton number and skin friction coefficient distributions from the present method and the viscous shock layer, and excellent agreement between the two methods is exhibited.

Figure 4 shows velocity and total enthalpy profile data from the two methods at a surface location of x/r_n = 15. The boundary-layer solution was terminated at a y location such that H/H_∞ had attained a value close to unity at y/y_e = 0.9; the shock layer data extend out to the computed location of the bow shock wave. These profile data also show good agreement between the two methods.

Figure 5 compares static pressure and normal velocity data from the present method and the shock layer method at x/r_n = 15. In addition, pressure data obtained using the inviscid method of characteristics treatment of Ref. 13 is shown. There is reasonable agreement, considering the expanded abscissa scale, among the three methods where they overlap; however, noting that Eq. (3) requires $\partial p/\partial y \geq 0$ for this case, it is obvious that the outer region of decreasing static pressure could not be obtained using this model for treating the flow in such a region. Obviously, as mentioned in Ref. 4, the static pressure variation shown here is negligibly small; it has been considered only for demonstrating the capability for treating it. The normal velocity data show good agreement between the present results and those obtained by the method of Ref. 12.

The results discussed in this subsection serve to validate the basic method which has been presented for treating laminar boundary-layer flows, and to demonstrate the capability (and some limitations) for computing the static pressure variation with y and the normal component of velocity in boundary-layer flows.

3.2 CONE-OGIVE-CYLINDER IN MACH 7.2 FLOW

In Refs. 14 and 15, Horstman and Owen present detailed measurements of the flow in the turbulent boundary layer on a slender cone-ogive-cylinder body in a Mach 7.2 flow. They report measurements of surface pressure, skin friction, and heating rate, profiles of various mean flow parameters, and results of hot-wire probe measurements. Figures 6 and 7 and Table 1 compare results from the present investigation with the data obtained by Hortsman and Owen for all except their hot-wire results.
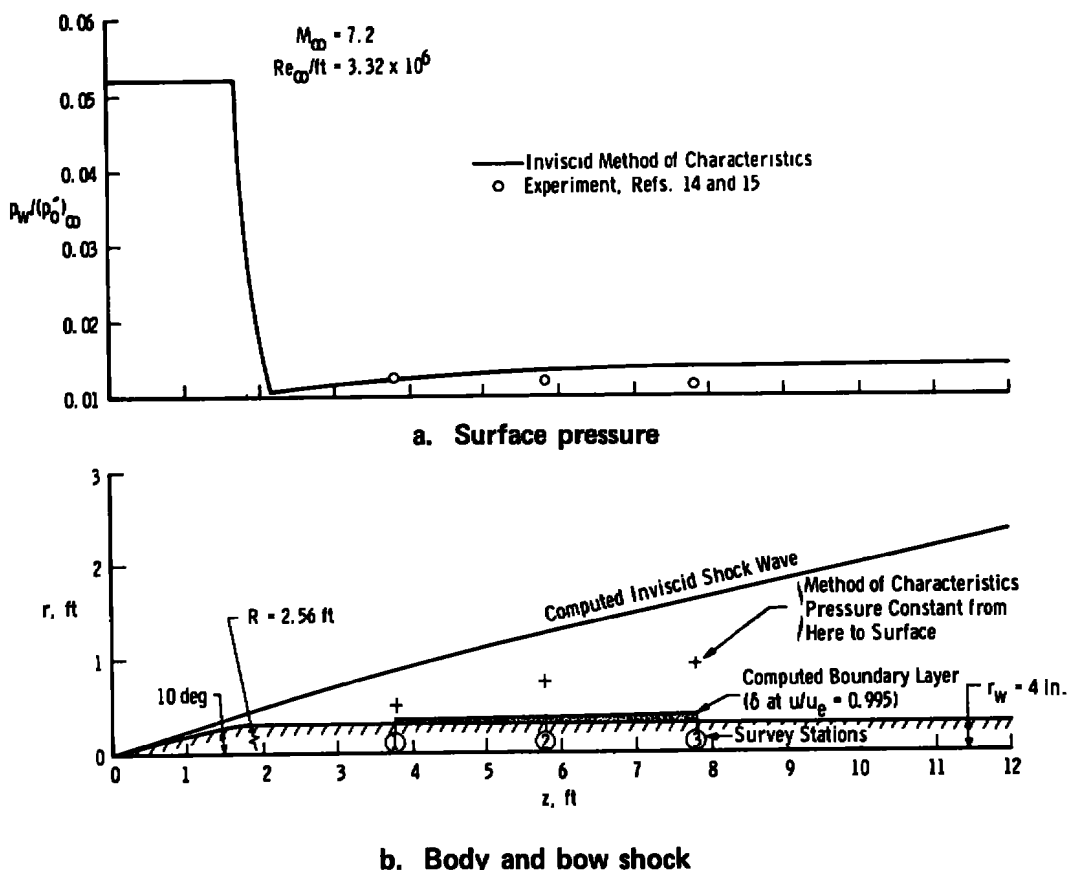

a. Surface pressure

b. Body and bow shock

Figure 6. Surface pressure distribution, body, and bow shock for cone-ogive-cylinder in a Mach 7.2 flow.
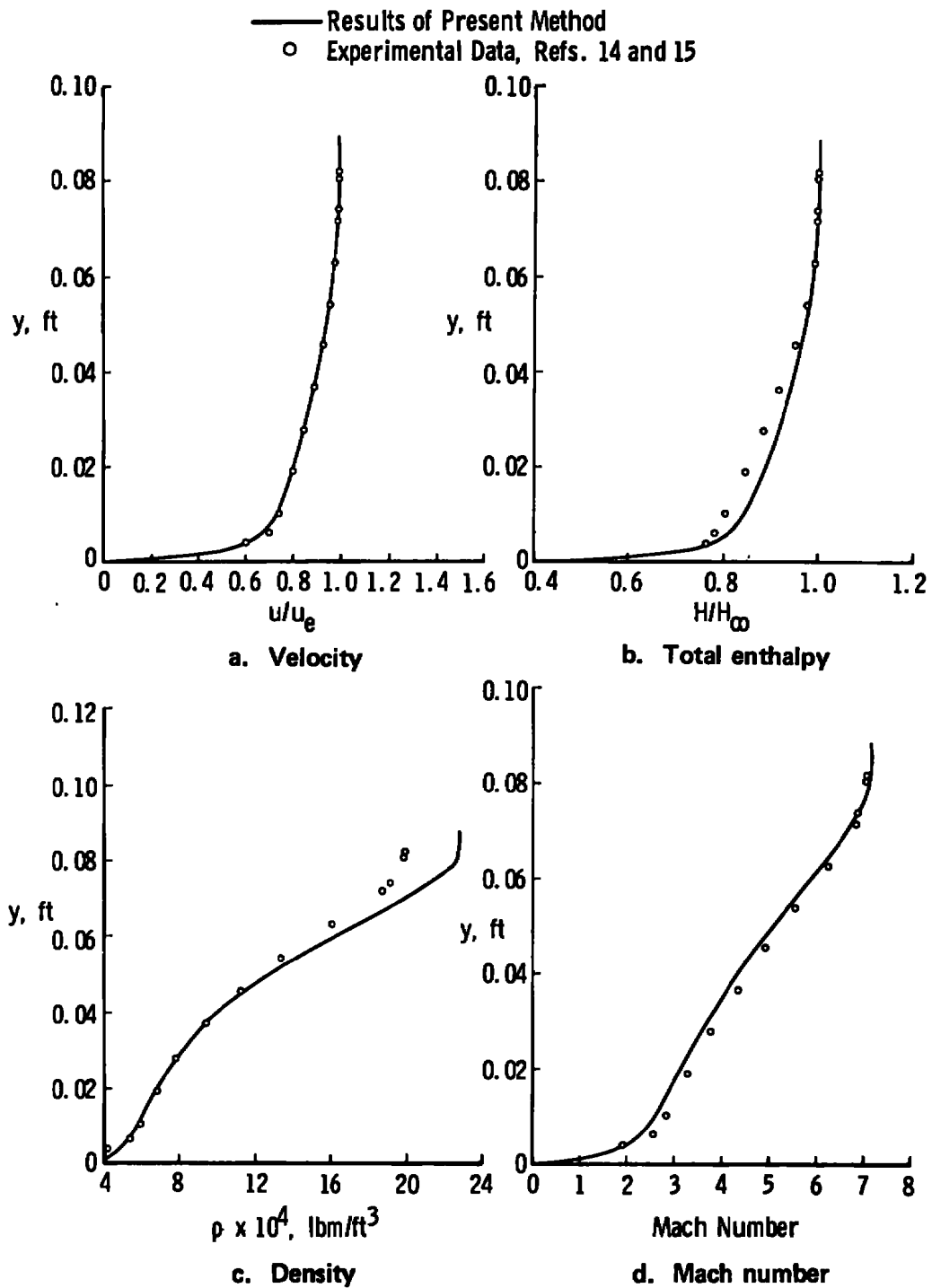
21

Figure 7. Boundary-layer profiles at Station 2 on cone-ogive-cylinder in a Mach 7.2 flow.

Table 1. Boundary-Layer Parameters for Cone-Ogive-Cylinder in a Mach 7.2 Flow

	Measured	Computed	Measured	Computed	Measured	Computed
Station	1	1	2	2	3	3
x, ft	3.80	3.80	5.80	5.80	7.80	7.80
δ, ft	0.0558	0.053	0.082	0.079	0.1083	0.104
δ^*, ft	0.0284	0.0287	0.0427	0.0432	0.0531	0.0557
θ, ft	0.00176	0.00174	0.00273	0.00271	0.00390	0.00360
$c_{f_e} \times 10^3$	0.90	0.884	0.855	0.854	0.801	0.835
$St_e \times 10^3$	0.510	0.612	0.458	0.569	0.484	0.543

Notes: 1. δ^*, θ include transverse curvature

2. $\delta - y$ at $p_0'/(p_0')_{y \to \infty} = 0.99$

3. $c_{f_e} = 2\tau_w/\rho_e u_e^2$

4. $St_e = \dot{q}_w/[\rho_e u_e(0.9 H_e - H_w)]$

The body was approximately 12 ft long, being basically a 4-in.-diam cylinder capped by a 10-deg half-angle cone followed by short ogive section; the cylinder began approximately 2 ft past the cone apex. The flow underwent transition from laminar to turbulent flow beginning at $x = 1.2$ ft and ending at $x = 2.6$ ft, and the surface-to-free-stream total-temperature ratio was 0.465.

Figure 6 shows the surface pressure distribution, the body shape, and the bow shock shape for the case of Horstman and Owen. The surface pressure distribution computed using the method of characteristics technique of Ref. 13 agrees reasonably well with the experimental data, although the computed value is about 10 percent higher than that measured at the last measuring point. In Fig. 6b, the computed boundary-layer thickness is seen to be less than 10 percent of the distance from the body to the bow shock at the locations where boundary-layer profile and surface heating rate and skin friction measurements were made. Also shown in Fig. 6b is the location (at each survey station) out to which the computed static pressure was essentially constant. Because the body longitudinal curvature is zero over the cylinder, the boundary-layer computations assumed $\partial p/\partial y = 0$ in that region. Inclusion of longitudinal curvature effects over the ogive section had no significant effect on the flow at the survey stations.

Table 1 compares boundary-layer thickness data, integral quantities, and surface heating and friction parameters as measured with those computed. The computed and experimentally determined thickness

and integral parameters are in excellent agreement. The computed coefficient of skin friction is within ±4 percent of the experimental data at each station. The computed Stanton number is approximately 20 percent greater than the experimental data; however, the experimental data do not show the expected monotonically decreasing behavior.

Figure 7 shows boundary-layer profiles at survey station 2. The comparisons between the computed results and the experimental data were very similar to these at all three survey stations, and these are presented as typical. There is good agreement between computation and experiment in the case of the velocity, total enthalpy, and Mach number profiles. The density profiles agree well except near the outer edge of the boundary layer, where the computed data reach a value almost 15 percent greater than that measured.

3.3 MACH 8 NOZZLE FLOW

In this section are presented comparisons between experimental data and computations for the case of supersonic flow in a nozzle. The experimental data were taken in the Arnold Engineering Development Center von Kármán Facility's Hypersonic Wind Tunnel B at an exit Mach number of approximately 8. The axisymmetric contoured nozzle is approximately 22 ft long, with a throat radius of 1.60 in. and an exit radius of about 2 ft. Tabulated geometry data are given in Ref. 16.

The test condition considered was one for which the total pressure was 605 psia and the total temperature 1321°R. At the survey station where the experimental data were taken, the unit Reynolds number outside the boundary layer was 2.69×10^6/ft, and the corresponding Mach number was 8.02. These data and the experimental data which will be presented were taken from Ref. 17. Surface temperature data used in the computations were taken from estimates given in Ref. 18.

The inviscid data which provided the boundary conditions used along the outer edge of the boundary layer were determined by an isentropic expansion from reservoir conditions to a known pressure at a given value of x. The pressure distribution (in x) was obtained from one-dimensional stream tube relationships. Viscous interaction effects were considered by forming an effective area distribution which took into account the boundary-layer displacement thickness. This required an iteration with respect to the displacement thickness, in a manner similar to that described in Ref. 19.

Figure 8 shows the results of the iteration procedure, beginning with an initial approximation to the displacement thickness distribution which was a bit high, and converging reasonably well in 2 iterations. Because of the difficulties in defining and computing a displacement (or momentum) thickness when considering longitudinal curvature and normal pressure gradient effects, these effects were neglected in these nozzle boundary-layer computations. (The initial boundary-layer solution was performed with and without the longitudinal curvature/normal pressure gradient effects, and the net effect on the solution was negligible.)
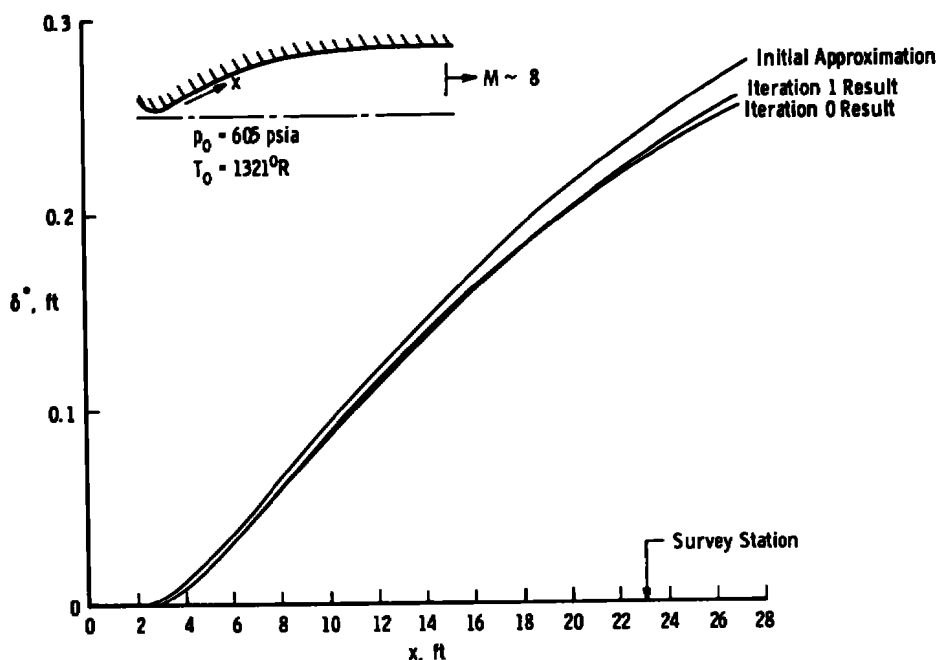
Figure 8. Displacement thickness iterations for Mach 8 nozzle case.

Table 2 lists the measured and computed displacement and momentum thickness values at the survey station. The computed displacement thickness is approximately fifteen percent greater than the experimentally inferred value, and the computed momentum thickness almost thirty percent less than the experimental value. It might be noted that the results of nozzle boundary-layer computations similar to the present ones were given in Ref. 20, and the general nature of the agreement between the computed and measured data was essentially as obtained in this investigation.

Table 2. Boundary-Layer Parameters at Exit of Mach 8 Nozzle

	δ^*, ft	θ, ft
Measured	0.198	0.0221
Computed	0.227	0.0160

Figure 9 shows comparisons between computed and measured impact pressure and total enthalpy profiles at the survey station. Reasonable agreement is shown between the computations and the experimental data. The computed profiles extend as far in y as the calculations were carried, while the experimental data actually continued beyond the region shown but with constant values of the pitot pressure and total enthalpy.
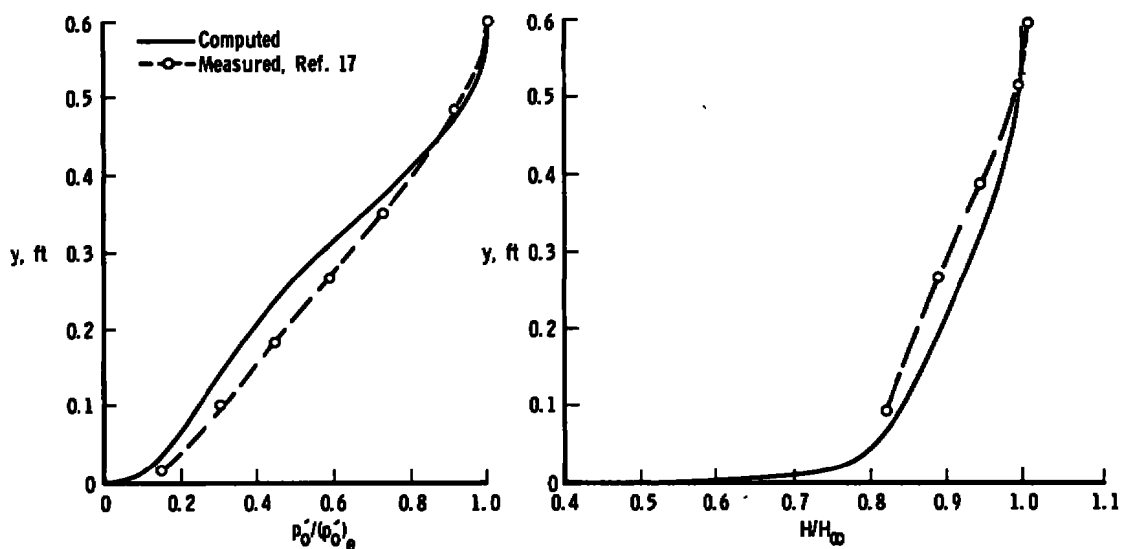
Figure 9. Impact pressure and total enthalpy profiles at exit of Mach 8 nozzle.

3.4 RAMP IN MACH 3.54 FLOW

In Ref. 21, Sturek presents the results of an experimental investigation of the turbulent boundary-layer flow over a two-dimensional isentropic compression ramp with significant longitudinal curvature and normal pressure gradient effects. The ramp was affixed to the floor of the test section of a supersonic wind tunnel adjusted to give a Mach 3.54 uniform flow approaching the ramp. The condition considered in this

study was one for which the total temperature was 560°R and the total
pressure was 48.34 psia. The ramp surface was essentially adiabatic,
and the test section boundary layer approaching the ramp was approxi-
mately 1 in. thick.

In order to begin the computations one-seventh power profiles of
u/u_e and $(H-H_w)/(H_e-H_w)$ were assumed, giving the comparison shown
in Fig. 10 between the assumed and measured velocity and total enthalpy
profiles approaching the ramp. The velocity profiles agree quite well,
and the total enthalpy profiles agree to within about 2 percent, although
the assumed profile does not exhibit the overshoot to be expected in the
outer region of the boundary layer on an adiabatic surface. At the
location where the computations were begun, the static pressure was
constant across the boundary layer.
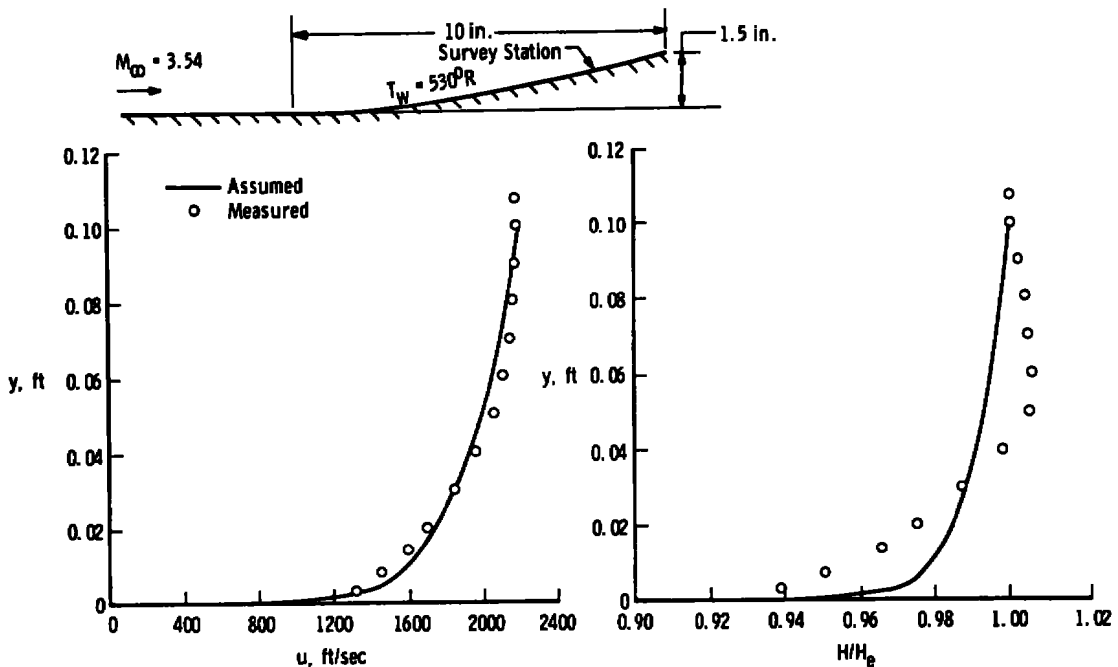
Figure 10. Assumed and measured profiles near the beginning of a ramp in
a Mach 3.54 flow.

The measured pressure distribution along the ramp was used to pro-
vide the necessary data for determining the inviscid flow over the ramp,
according to the scheme discussed in Section 2.1. The coordinates of the
ramp were fitted by a curve of the form $y = ax^b$ (where x and y are rec-
tangular cartesian coordinates), and the corresponding longitudinal radius
of curvature was determined analytically.

Figure 11 shows computed and measured profiles of velocity, total enthalpy, and static pressure at a survey station approximately 8 in. back on the ramp.
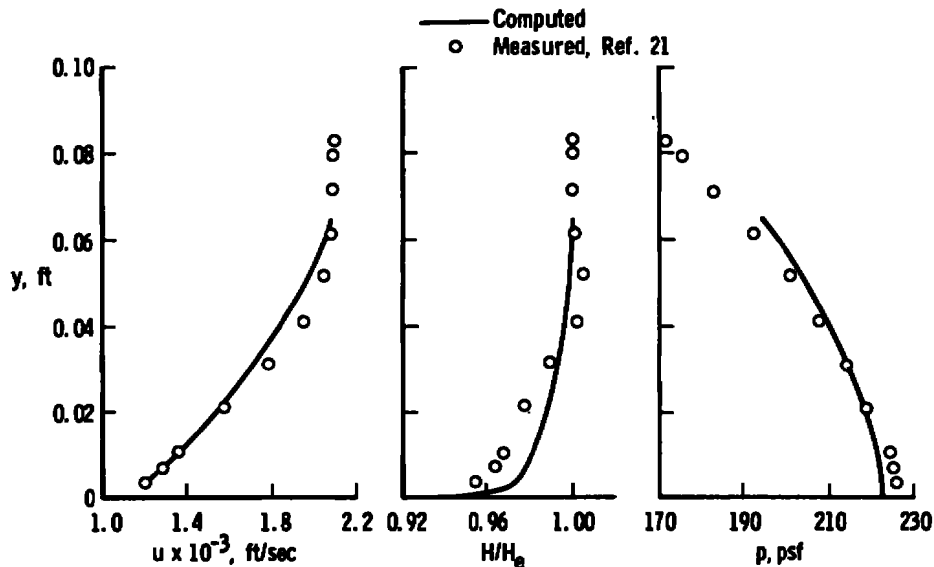
Figure 11. Computed and measured velocity, total enthalpy, and static pressure profiles at survey station on ramp in a Mach 3.54 flow.

Good agreement is shown between the measured and computed data, except that the computed total enthalpy profile still shows no overshoot. In particular, the static pressure variation is felt to be quite well represented by the model used in the computations.

Figure 12 compares computed and measured surface shearing stress distributions along the ramp. The two sets of data agree reasonably well, but the experimental data increase less rapidly over the forward portion of the ramp and more rapidly over the aft portion of the ramp than the computed shearing stress.

Figure 12. Computed and measured surface shearing stress distribution on ramp in a Mach 3.54 flow.
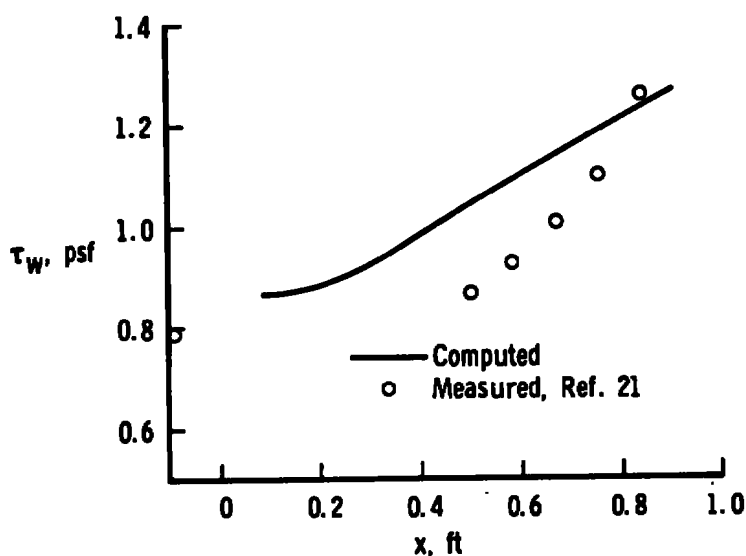
4.0 SUMMARY AND CONCLUSIONS

The compressible laminar and turbulent boundary-layer equations for two-dimensional and axisymmetric flow have been presented in a form which includes transverse curvature, longitudinal curvature, and normal pressure gradient effects. The equations were first presented in physical surface coordinates and then transformed using the ω^2 transformation to a form for which a finite-difference solution procedure was developed. The stagnation point form of the boundary-layer equations in x-ω coordinates was also presented, to the author's knowledge the first time this has been done.

The method presented for treating boundary-layer flows was tested by comparing results from the present method with both experimental data and results from other methods of calculation. Generally good agreement was obtained for a variety of cases, including both internal and external boundary layers and a case in which normal pressure gradient and longitudinal curvature effects were significant.

The method presented herein would be difficult to apply to situations in which boundary-layer displacement influences needed to be considered. This is because of the difficulty which would be encountered in defining

and computing a displacement thickness when normal pressure gradient and longitudinal curvature effects were included. The best approach for such cases would be the development of a fully viscous shock layer method of more general applicability than that given in Ref. 12.

REFERENCES

1. Patankar, S. V. and Spalding, D. B. Heat and Mass Transfer in Boundary Layers, CRC Press, Cleveland, Ohio, 1968.

2. Mayne, A. W., Jr. and Dyer, D. F. "Comparisons of Theory and Experiment for Turbulent Boundary Layers on Simple Shapes at Hypersonic Conditions." Proceedings of the 1970 Heat Transfer and Fluid Mechanics Institute, Stanford University Press, 1970, pp. 168-188.

3. Whitfield, D. L. "Viscous Effects in Low-Density Nozzle Flows." AEDC-TR-73-52 (AD761489), June 1973.

4. Mayne, A. W., Jr. and Adams, J. C., Jr. "Streamline Swallowing by Laminar Boundary Layers in Hypersonic Flow." AEDC-TR-71-32 (AD719748), March 1971.

5. Dyer, D. F. "Modification of the Patankar-Spalding Two-Dimensional Boundary Layer Calculation Procedure for Three-Dimensional Windward Streamline Plane." ONR London Report R-20-73 (AD772706), September 1973.

6. Landis, R. B. "Numerical Solution of Variable Property Turbulent Boundary Layers with Foreign Gas Injection." Ph. D. Dissertation, University of California, Los Angelas, 1971.

7. Denny, V. E. and Landis, R. B. "An Improved Transformation of the Patankar-Spalding Type for Numerical Solution of Two-Dimensional Boundary Layer Flows." International Journal of Heat and Mass Transfer, Vol. 14, 1971, pp. 1859-1862.

8. Cohen, N. B. "Correlation Formulas and Tables of Density and Some Transport Properties of Equilibrium Dissociating Air for Use in Solutions of the Boundary-Layer Equations." NASA TN D-194, February 1960.

9. Maslen, S. H. "Second-Order Effects in Laminar Boundary Layers." AIAA Journal, Vol. 1, No. 1, January 1963, pp. 33-40.

10. Back, L. H. "Transonic Laminar Boundary Layers with Surface Curvature." International Journal of Heat and Mass Transfer, Vol. 16, 1973, pp. 1745-1761.

11. Dhawan, S. and Narasimha, R. "Some Properties of Boundary Layer Flow during the Transition from Laminar to Turbulent Motion." Journal of Fluid Mechanics, Vol. 3, No. 4, 1958, pp. 418-436.

12. Davis, R. T. "The Hypersonic Fully Viscous Shock-Layer Problem." Report SC-RR-68-840, Sandia Corporation, Albuquerque, New Mexico, 1968. See also AIAA Journal, Vol. 8, No. 5, May 1970, pp. 843-851.

13. Inouye, M., Rakich, J. V., and Lomax, H. "A Description of Numerical Methods and Computer Programs for Two-Dimensional and Axisymmetric Supersonic Flow over Blunt-Nosed and Flared Bodies." NASA TN D-2970, August 1965.

14. Horstman, C. C. and Owen, F. K. "Turbulent Properties of a Compressible Boundary Layer." AIAA Journal, Vol. 10, No. 11, November 1972, pp. 1418-1424.

15. Owen, F. K. and Horstman, C. C. "On the Structure of Hypersonic Turbulent Boundary Layers." Journal of Fluid Mechanics, Vol. 53, No. 4, 1972, pp. 611-636.

16. Fitch, C. R. "Flow Quality Improvement at Mach 8 in the VKF 50-in. Hypersonic Wind Tunnel B." AEDC-TR-66-82 (AD632828), May 1966.

17. Matthews, R. K. and Trimmer, L. L. "Nozzle Turbulent Boundary-Layer Measurements in the VKF 50-in. Hypersonic Tunnels." AEDC-TR-69-118 (AD854309), June 1969.

18. Sivells, J. C. "Aerodynamic Design and Calibration of the VKF 50-in. Hypersonic Wind Tunnels." AEDC-TDR-62-230 (AD299774), March 1963.

19. Whitfield, D. L. "Theoretical and Experimental Investigation of Boundary Layers in Low Density Hypersonic Axisymmetric Nozzles." AEDC-TR-68-193 (AD674597), September 1968.

20. Bushnell, D. M., et al. "Comparison of Prediction Methods and Studies of Relaxation in Hypersonic Turbulent Nozzle-Wall Boundary Layers." Compressible Turbulent Boundary Layers, NASA SP-216, December 1968.

21. Sturek, W. B. "An Experimental Investigation of the Supersonic Turbulent Boundary Layer in a Moderate Adverse Pressure Gradient. Part I. A Detailed Description of the Experiment and Data Tabulation." Ballistic Research Laboratories Report 1506, October 1970.

NOMENCLATURE

A, B, C, D, P	Terms in finite-difference equations
A^*	Mixing length constant
a, b, c, d	Terms in general form of governing equations
c_{f_e}	Edge skin friction coefficient, $2\tau_w/\rho_e u_e^2$
c_{f_∞}	Free-stream skin friction coefficient, $2\tau_w/\rho_\infty U_\infty^2$
f	General variable, especially u or H
H	Stagnation enthalpy
k	Mixing length constant
M	Mach number
$\dot{m}''$	Mass flux term
N	Number of cross-stream grid points
PEI	$\psi_e - \psi_w$
p	Pressure
p_o'	Pitot pressure
Pr	Prandtl number
$\dot{q}$	Heat-transfer rate
R	Longitudinal radius of curvature
Re_∞, r_n	Free-stream Reynolds number based on nose radius
r	Radial coordinate
r_n	Nose radius of curvature
St_e	Edge Stanton number
St_∞	Free-stream Stanton number, $\dot{q}_w/\rho_\infty U_\infty(H_\infty - H_w)$
T	Temperature
T'	Terms in stagnation point equations
U_∞	Free-stream velocity
u	Velocity in x direction
v	Velocity in y direction

x	Coordinate along the surface
y	Coordinate normal to the surface
y_m	Value of y at $u/u_e = 0.99$
z	Axial distance
γ	Intermittency factor
δ	Boundary-layer thickness
δ^*	Boundary-layer displacement thickness
ζ	u/u_e
θ	Momentum thickness
κ	Longitudinal curvature, $1/R$
λ	Mixing length constant
μ	Viscosity
ρ	Mass density
τ	Shearing stress
ϕ	Surface slope
ψ	Stream function
ω	Transformed stream function

SUBSCRIPTS

e	Outer edge of boundary layer
ℓ	Laminar
t	Turbulent
w	Wall or surface
o	Stagnation conditions
∞	Free-stream, or reservoir for internal flow